Adiabatic hyperspherical study of weakly bound helium–helium–alkali-metal triatomic systems

Hiroya Suno[1,*] and B. D. Esry[2]

[1]*The Earth Simulator Center, Japan Agency for Marine-Earth Science and Technology, 3173-25 Showa-machi,
Kanazawa-ku, Yokohama 236-0001, Japan*
[2]*Department of Physics, Kansas State University, Manhattan, Kansas 66506, USA*
(Received 14 October 2010; published 29 December 2010)

^{4}He$_2$–alkali-metal triatomic molecular systems are studied using the adiabatic hyperspherical representation. By adopting the best pairwise He-He and He-X interaction potentials, we search for weakly bound states of ^{4}He$_2X$ systems with $X =$ ^{6}Li, ^{7}Li, ^{23}Na, ^{39}K, ^{40}K, ^{41}K, ^{85}Rb, ^{87}Rb, and ^{133}Cs. We consider not only zero total angular momentum $J = 0$ states, but also $J > 0$ states. We find that the ^{4}He$_2^6$Li and ^{4}He$_2^7$Li systems each possess two bound states with $J^\Pi = 0^+$ symmetry and none with $J > 0$, while the other ^{4}He$_2$–alkali-metal species are found to support one 0^+ and one 1^- bound state. We calculate the bound-state energies of these molecular species and discuss the essential features of the wave functions associated with these bound states.

I. INTRODUCTION

Triatomic helium systems have been attracting considerable interest due to the possibility of observing very weakly bound states, since the ^{4}He dimer supports one and only one very weakly bound state whose binding energy is on the order of millikelvins. Several sophisticated helium dimer interaction potentials have been developed, such as the LM2M2 potential by Aziz and Slaman [1], and the HFD-B3-FCI1 potential by Aziz *et al.* [2]. Recently, Jeziorska *et al.* [3] and Cencek *et al.* [4] proposed not only a helium dimer potential, but also the nonadditive three-body term. All of these potentials have been used to calculate various properties of the helium dimer and trimer (and their isotopes) [5–9] as well as their scattering observables [9–16]. On the other hand side, since the ^{4}He dimer is so weakly bound and is thus difficult to detect, it was not until 1993 that experimental evidence for the existence of a dimer bound state was obtained by Luo *et al.* [17,18]. Simultaneously, Schöllkopf and Toennies [19,20] measured not only the helium dimer, but also the trimer and tetramer. The system was revisited more recently in Refs. [21–23].

In addition to the well-studied helium dimers and trimers, there exist other examples of weakly bound diatomic and triatomic molecules that have binding energies of the order of 1 K or less. Indeed, the interaction potentials between He and alkali-metal atoms are also found to have a very shallow well. These potentials have been investigated since the 1970s by Dehmer and Wharton [24] in scattering experiments. Theoretically, the interaction potentials for helium–alkali-metal systems were obtained by Cvetko *et al.* [25] and Kleinekathöfer *et al.* [26,27]. It turns out that He–alkali-metal potentials are even shallower than the He-He potential, and one may find weakly bound diatomic molecules HeX and triatomic molecules He$_2X$ ($X =$ alkali-metal atom) with binding energies as small as those of the helium-only systems. Using these helium–alkali potentials mentioned above, several theoretical investigations have been carried out for He$_2X$ systems. Searching for weakly bound triatomic molecules,

Yuan and Lin [28] studied the He$_2$Li and He$_2$Na systems and found ground states bound by less than 1 K. In a later study, Delfino *et al.* [29] investigated the same systems and predicted the existence of an excited state, whose energy is close to -2.31 mK, for the ^{4}He$_2^7$Li system. Baccarelli *et al.* [30,31] confirmed the existence of, and studied the location and spatial shape for, the ground and excited states of the ^{4}He$_2^6$Li and ^{4}He$_2^7$Li systems. The ground states of ^{4}He$_2^7$Li and ^{4}He$_2^{23}$Na were also considered by Di Paola *et al.* [32]. On the other hand, Li *et al.* [33] found one bound state each for ^{4}He$_2^{39}$K, ^{4}He^{3}He^{39}K, and ^{3}He$_2^{39}$K. Among the He–He–alkali-metal systems, the heavier alkali-metal atoms, Rb and Cs, have not been considered yet.

In this work, we study the bound states of ^{4}He$_2$–alkali-metal triatomic molecules, extending the previous investigations in Refs. [28–33]. We consider all the alkali-metal species, that is, ^{6}Li, ^{7}Li, ^{23}Na, ^{39}K, ^{40}K, ^{41}K, ^{85}Rb, ^{87}Rb, and ^{133}Cs. In addition, we treat not only zero total nuclear orbital angular momentum, i.e., $J = 0$ states, but also $J > 0$ states. Note that none of these previous investigations [28–30,33] treated rotational bound states of these systems. We calculate all the existing bound-state energies for the ^{4}He$_2$–alkali-metal triatomic molecules. The key ingredient in our numerical calculations is the adiabatic hyperspherical representation [5,14,34]. Enforcing the boson permutation symmetry is greatly simplified using a modified version of the Smith-Whitten hyperspherical coordinate system [14,35,36].

We adopt the sum of the relevant pairwise potentials for the total interaction. For the helium-helium interaction, we use the representation of Jeziorska *et al.* [3], while the potential of Kleinekathöfer *et al.* [27] is employed for the interaction between helium and alkali-metal atoms. The scattering lengths a and characteristic lengths r_0, calculated from these potentials, satisfy the so-called universality requirement ($a/r_0 \gg 1$) for the ^{4}He-^{4}He system ($a/r_0 \approx 16$) but not for the ^{4}He–alkali-metal systems ($a/r_0 \approx 4$). These interaction potentials can also be used to calculate the three-body recombination rates [37] and the atom-diatom scattering cross sections [38].

This paper is organized as follows. We explain our method and give all necessary formulas for calculating the bound-state energies of the ^{4}He$_2$–alkali-metal systems in Sec. II. The

———————
*suno@jamstec.go.jp

results are presented in Sec. III. A summary of this work is given in Sec. IV. We use atomic units throughout except where explicitly stated otherwise.

II. METHOD

We solve the Schrödinger equation for three interacting atoms using the adiabatic hyperspherical representation [5,9,14,34]. In the adiabatic hyperspherical representation, we calculate eigenfunctions and eigenvalues of the fixed-hyperradius Hamiltonian in order to construct a set of coupled radial equations. The bound-state energies can be obtained as the discrete eigenvalues from these coupled equations. Since the method employed is largely the same as detailed in Refs. [9], [14], and [37], we give only a brief outline here.

After separation of the center-of-mass motion, the three-body problem can be described by six coordinates. Three of these can be chosen as the Euler angles, α, β, and γ, that specify the orientation of the body-fixed frame relative to the space-fixed frame. The remaining three internal coordinates can be represented by a hyperradius R and two hyperangles θ and φ. To define these internal coordinates, we use a slightly modified version of the Smith-Whitten hyperspherical coordinates [9,14,35,36,39,40]. The hyperspherical coordinates $(R,\Omega) \equiv (R,\theta,\varphi,\alpha,\beta,\gamma)$ used in this work are defined in Ref. [9].

In terms of a rescaled wave function ψ_n, which is related to the usual Schrödinger solution Ψ_n by $\psi_n = R^{5/2}\Psi_n$ (the volume element relevant to integrals over $|\psi_n|^2$ becomes $2dR \sin 2\theta d\theta d\varphi d\alpha \sin \beta d\beta d\gamma$), the nuclear Schrödinger equation for three particles interacting through the potential $V(R,\theta,\varphi)$ reads

$$\left[-\frac{1}{2\mu}\frac{\partial^2}{\partial R^2} + \frac{\Lambda^2 + 15/4}{2\mu R^2} + V(R,\theta,\varphi) \right]\psi_n = E_n\psi_n, \quad (1)$$

where μ is the three-body reduced mass and is given by

$$\mu^2 = \frac{m_1 m_2 m_3}{m_1 + m_2 + m_3}, \quad (2)$$

with m_i ($i = 1,2,3$) being the mass of particle i. The masses of the atoms used in this work are listed in Table I. In our

TABLE I. Masses of the atoms used in this work. Relative atomic masses, or masses in units of u, are those defined with respect to the ^{12}C atomic mass being 12 and are taken from the NIST Element Data Index [42]. Masses in atomic units (a.u.) are obtained by dividing them by the electron mass in u, $m_e = 5.485\,799\,094\,3 \times 10^{-4}$ u.

Atom	Relative atomic mass	Mass (a.u.)
^{4}He	4.002 603 25	7296.299 37
^{6}Li	6.015 122 79	109 64.8981
^{7}Li	7.016 004 55	127 89.3939
^{23}Na	22.989 769 28	419 07.785 69
^{39}K	38.963 706 68	710 26.492 24
^{40}K	39.963 998 48	728 49.912 64
^{41}K	40.961 825 76	746 68.840 50
^{85}Rb	84.911 789 74	154 784.723 76
^{133}Cs	132.905 451 93	242 271.817 916
^{87}Rb	86.909 180 53	158 425.744 43

convention, we designate the alkali-metal atom as particle 1 and the ^{4}He atoms as particles 2 and 3. In expression (1), Λ^2 is the squared grand angular momentum operator. In our calculations, the first step consists of solving the fixed-R adiabatic eigenvalue equation for a given set of quantum numbers J (total nuclear orbital angular momentum), M (its projection on a laboratory-fixed axis), and Π (parity with respect to the inversion of the nuclear coordinates),

$$\left[\frac{\Lambda^2 + 15/4}{2\mu R^2} + V(R,\theta,\varphi) \right]\Phi_\nu(R;\Omega) = U_\nu(R)\Phi_\nu(R;\Omega), \quad (3)$$

to obtain the channel functions $\Phi_\nu(R;\Omega)$ and the potential curves $U_\nu(R)$. The adiabatic eigenfunction expansion gives the total wave function ψ_n in terms of the complete, orthonormal set of angular wave functions Φ_ν and radial wave functions $F_{\nu n}$,

$$\psi_n(R,\Omega) = \sum_\nu F_{\nu n}(R)\Phi_\nu(R;\Omega), \quad (4)$$

where ν is a collective index that includes all the quantum numbers necessary to identify each channel. If the expansion in Eq. (4) includes the complete, infinite set of Φ_ν, this representation of ψ_n is exact. In practice, the sum is truncated to a finite number of terms but can be extended systematically to obtain any desired level of accuracy. The adiabatic equation in Eq. (3) is solved by further expanding the channel functions on Wigner rotation matrices D_{KM}^J,

$$\Phi_\nu(R;\Omega) = \sum_K \phi_{K\nu}(R;\theta,\varphi)D_{KM}^J(\alpha,\beta,\gamma), \quad (5)$$

where K takes the values $J, J-2, \ldots, -(J-2), -J$ for the party-favored case, $\Pi = (-1)^J$, and $J-1, J-3, \ldots, -(J-3), -(J-1)$ for the parity-unfavored case, $\Pi = (-1)^{J+1}$. The remaining degrees of freedom are solved by expanding $\phi_{K\nu}(R;\theta,\varphi)$ onto a direct product of fifth-order basis splines [41] in θ and φ.

Insertion of ψ_n from Eq. (4) into the Schrödinger equation from Eq. (1) results in a set of coupled ordinary differential equations:

$$\left[-\frac{1}{2\mu}\frac{d^2}{dR^2} + U_\nu(R) - \frac{1}{2\mu}Q_{\nu\nu}(R) \right]F_{\nu n}(R)$$
$$- \frac{1}{2\mu}\sum_{\nu'\neq\nu}\left[2P_{\nu\nu'}(R)\frac{d}{dR} + Q_{\nu\nu'}(R) \right]F_{\nu' n}(R) = E_n F_{\nu n}(R). \quad (6)$$

The coupling elements $P_{\nu\nu'}(R)$ and $Q_{\nu\nu'}(R)$ involve partial first and second derivatives of the channel functions Φ_ν with respect to R and are defined as

$$P_{\nu\nu'}(R) = \left\langle\!\!\left\langle \Phi_\nu(R) \left| \frac{\partial}{\partial R} \right| \Phi_{\nu'}(R) \right\rangle\!\!\right\rangle, \quad (7)$$

and

$$Q_{\nu\nu'}(R) = \left\langle\!\!\left\langle \Phi_\nu(R) \left| \frac{\partial^2}{\partial R^2} \right| \Phi_{\nu'}(R) \right\rangle\!\!\right\rangle. \quad (8)$$

The double-bracket matrix element signifies that integrations are carried out only over the angular coordinates Ω. The bound-state energies $E_n^{J\Pi}(n = 0,1,\ldots)$ can be obtained as
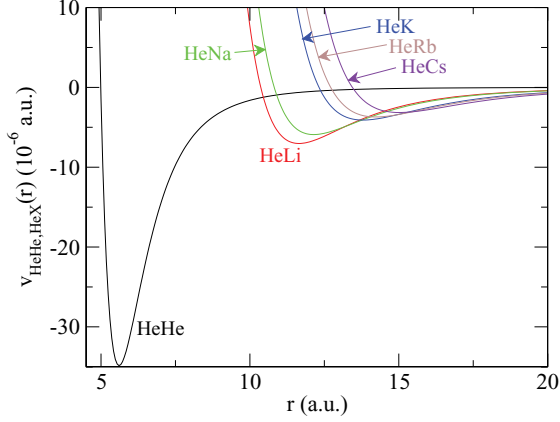
FIG. 1. (Color online) Pairwise interaction potentials for He-He and He-X (X = alkali-metal atom).

TABLE II. Bound-state energies E_{00} (1 a.u. $= 3.157\,746\,5 \times 10^8$ mK) and scattering lengths a for the ^{4}He-^{4}He and ^{4}He–alkali-metal systems.

	E_{00} (a.u.)	E_{00} (mK)	a (a.u.)	a (Å)
^{4}He$_2$	-5.472×10^{-9}	-1.728	165.4	87.53
^{4}He$_2$[a]	-4.148×10^{-9}	-1.310	189.0	100.01
^{4}He^{6}Li	-4.797×10^{-9}	-1.515	169.0	89.43
^{4}He^{7}Li	-1.780×10^{-8}	-5.622	92.29	48.84
^{4}He^{7}Li[b]	-8.883×10^{-9}	-2.805	124.8	66.04
^{4}He^{23}Na	-9.178×10^{-8}	-28.98	44.14	23.36
^{4}He^{39}K	-3.547×10^{-8}	-11.20	62.96	33.32
^{4}He^{40}K	-3.618×10^{-8}	-11.42	62.44	33.04
^{4}He^{41}K	-3.686×10^{-8}	-11.64	61.96	32.79
^{4}He^{85}Rb	-3.253×10^{-8}	-10.27	64.27	34.01
^{4}He^{87}Rb	-3.282×10^{-8}	-10.36	64.04	33.41
^{4}He^{133}Cs	-1.566×10^{-8}	-4.945	85.63	45.31

[a]Using the He-He potential from Ref. [1].
[b]Using the Li-He potential from Ref. [25].

the discrete eigenenergies from the coupled equations in Eq. (6).

The interaction potential $V(R,\theta,\varphi)$ used in this work is expressed as a sum of three pairwise potentials,

$$V(R,\theta,\varphi) = v_{\mathrm{He}X}(r_{12}) + v_{\mathrm{HeHe}}(r_{23}) + v_{\mathrm{He}X}(r_{31}), \quad (9)$$

where r_{ij} are the interparticle distances. In terms of hyperspherical coordinates, these are expressed as

$$r_{ij} = 2^{-1/2} d_{ij} R[1 + \sin\theta\cos(\varphi + \varphi_{ij})]^{1/2}, \quad (10)$$

with $\varphi_{12} = 2\tan^{-1}(m_2/\mu)$, $\varphi_{23} = 0$, $\varphi_{31} = -2\tan^{-1}(m_3/\mu)$, and

$$d_{ij}^2 = \frac{(m_k/\mu)(m_i + m_j)}{m_i + m_j + m_k}, \quad (11)$$

where the indices (i,j,k) are a cyclic permutation of $(1,2,3)$. For the helium dimer potential $v_{\mathrm{HeHe}}(r)$, we use the representation of Jeziorska *et al.* [3]; and for the helium–alkali-metal interactions $v_{\mathrm{He}X}(r)$, the potentials of Kleinekathöfer *et al.* [27]. These two-body potentials are shown in Fig. 1. For the ^{4}He$_2^7$Li system, we also employ the He-He potential of Aziz and Slaman [1] and the Li-He potential of Cvetko *et al.* [25] for the sake of comparison with the previous calculations in Refs. [30] and [31], which use these potentials, so that we can see the discrepancies due to the computational method. The ^{4}He$_2$ and ^{4}HeX bound-state energies $E_{v=0,l=0}$ and the scattering lengths a calculated from all these interaction potentials are summarized in Table II. These values agree well with the ones given in Ref. [3] and [27]. Note that all the ^{4}He–alkali-metal molecules, except ^{4}He^{6}Li, have larger binding energies $|E_{00}|$ than the ^{4}He$_2$ dimer—and thus smaller scattering lengths—moving them further from the universal regime.

In practice, we solve the adiabatic equation, (3), for a set of more than 180 radial grid points R_i up to $R \approx 2000$–4000 a.u. to obtain the potential curves $U_v(R)$ and the coupling matrix elements $P_{vv'}(R)$ and $Q_{vv'}(R)$. In solving the adiabatic equation, (3), we generate the basis splines for θ from 100 mesh points, while we use 120 mesh points for φ.

III. RESULTS AND DISCUSSION

For the parity-unfavored cases $\Pi = (-1)^{J+1}$, all the adiabatic hyperspherical potential curves are found to be repulsive and no bound state may exist. We hence limit our consideration only to the parity-favored cases $\Pi = (-1)^J$, that is, $J^\Pi = 0^+$, $1^-,\ldots$. For each of these symmetries, the lowest potential curve $v = 0$ corresponds asymptotically to ^{4}He$X + {}^4$He—a ^{4}He–alkali-metal molecule and a ^{4}He atom far away-while the second lowest one, $v = 1$, correlates with ^{4}He$_2 + X$—a ^{4}He dimer and an alkali-metal atom far away. These potential curves asymptotically ($R \to \infty$) behave as

$$U_0(R) - \frac{1}{2\mu} Q_{00}(R) \to E_{00}^{^4\mathrm{He}X} + \frac{J(J+1)}{2\mu R^2} \quad (12)$$

and

$$U_1(R) - \frac{1}{2\mu} Q_{11}(R) \to E_{00}^{^4\mathrm{He}_2} + \frac{J(J+1)}{2\mu R^2}, \quad (13)$$

where $E_{00}^{^4\mathrm{He}X}$ and $E_{00}^{^4\mathrm{He}_2}$ are the bound-state energies of ^{4}HeX and ^{4}He$_2$, respectively. This behavior holds for all the ^{4}He$_2$–alkali-metal systems except ^{4}He$_2^6$Li. For the latter system, the potential curves in Eqs. (12) and (13) are reversed in order, and the lowest and second-lowest ones correspond asymptotically to ^{4}He$_2 + {}^6$Li and ^{4}He^{6}Li $+ {}^4$He, respectively. All the higher channels, $v = 2,3,4,\ldots$, for each symmetry correspond asymptotically to three-body continuum states, i.e., all three atoms far away from each other as $R \to \infty$. We recall that in the adiabatic hyperspherical representation the three-body continuum is rigorously discretized since the adiabatic Hamiltonian depends only on the bounded hyperangles. These three-body continuum channel functions converge asymptotically to the hyperspherical harmonics. The corresponding potential curves therefore behave as

$$U_v(R) \to \frac{\lambda(\lambda + 4) + \frac{15}{4}}{2\mu R^2}, \quad \text{for} \quad R \to \infty. \quad (14)$$

In principle, λ can take on any non-negative integer value, but its possible values are restricted by the requirements

TABLE III. Bound-state energies of ^{4}He$_2$–alkali-metal molecules at various levels of approximation. Energies are given in units of millikelvins and are relative to the three-body dissociation threshold. For $\nu_{max} \to \infty$, energies measured relative to the lowest atom-molecule dissociation threshold, or binding energies, are also shown.

	J^Π	n	BO	Adiabatic	$\nu_{max}=5$	$\nu_{max}=10$	$\nu_{max}=20$	$\nu_{max}\to\infty$	$\nu_{max}\to\infty^{a}$
^{4}He$_2^6$Li	0^+	0	−117.53	−45.33	−57.05	−57.95	−58.42	−58.88	−57.36
		1	−2.80	−1.89	−2.07	−2.08	−2.09	−2.09	−0.58
^{4}He$_2^7$Li	0^+	0	−147.96	−63.59	−78.90	−80.03	−80.62	−81.29	−75.67
		1	−6.74	—^{b}	−5.65	−5.65	−5.66	−5.67	−0.04
^{4}He$_2^7$Li^c	0^+	0	−120.13	−51.15	−62.75	−63.56	−64.08	−64.26	−61.46
		1	−3.81	−2.86	−2.98	−2.99	−3.00	−3.01	−0.21
^{4}He$_2^{23}$Na	0^+	0	−217.28	−133.97	−148.90	−151.53	−152.32	−152.68	−123.70
	1^-	0	−113.95	−50.91	−57.96	−60.60	−61.39	−61.99	−33.00
^{4}He$_2^{39}$K	0^+	0	−127.66	−79.33	−87.32	−88.96	−89.44	−89.76	−78.56
	1^-	0	−61.58	−25.94	−29.30	−30.84	−31.43	−31.93	−20.73
^{4}He$_2^{40}$K	0^+	0	−128.49	−80.06	−88.08	−89.73	−90.22	−90.68	−79.26
	1^-	0	−62.53	−26.64	−30.06	−31.62	−32.25	−32.67	−21.25
^{4}He$_2^{41}$K	0^+	0	−129.28	−80.75	−88.81	−90.48	−90.97	−91.12	−79.48
	1^-	0	−63.44	−27.31	−30.78	−32.55	−33.20	−33.50	−21.86
^{4}He$_2^{85}$Rb	0^+	0	−118.17	−75.48	−82.52	−84.07	−84.49	−84.69	−74.42
	1^-	0	−61.40	−28.52	−31.80	−33.22	−33.94	−34.37	−24.10
^{4}He$_2^{87}$Rb	0^+	0	−118.52	−75.76	−82.84	−84.39	−84.81	−84.96	−74.60
	1^-	0	−61.80	−28.82	−32.11	−33.54	−34.26	−34.46	−24.10
^{4}He$_2^{133}$Cs	0^+	0	−87.74	−54.90	−60.15	−61.33	−61.64	−61.77	−56.83
	1^-	0	−40.95	−16.93	−19.10	−19.92	−20.55	−20.63	−15.69

^{a}Energies measured relative to the lowest atom-molecule dissociation threshold.
^{b}No state is found below the lowest atom-molecule dissociation threshold.
^{c}Using the He-He potential from Ref. [1] and the Li-He potential from Ref. [25].

of permutation symmetry [43]. The calculated adiabatic potential curves and nonadiabatic couplings are found to be accurate to three or four significant digits.

The "adiabatic approximation" corresponds to solving Eq. (6) with only one channel ν, where the sum over ν' is eliminated on the left-hand side. This leaves a one-dimensional Schrödinger equation with an effective hyper-radial potential $U_\nu(R) - \frac{1}{2\mu} Q_{\nu\nu}(R)$ that determines the three-body spectrum in the adiabatic approximation. The lowest energy level with $\nu = 0$ obtained by solving Eq. (6) neglecting all nondiagonal coupling elements gives a variational upper bound to the exact $n = 0$ state energy $E_0^{J^\Pi}$. One can also solve Eq. (6) by further neglecting the diagonal coupling term $Q_{\nu\nu}(R)$, which is the hyperspherical equivalent of the Born-Oppenheimer (BO) approximation. The lowest $\nu = 0$ energy level thus obtained gives a rigorous lower bound to the exact $n = 0$ state energy $E_0^{J^\Pi}$. Finally, solving Eq. (6) with the sums truncated at ν_{max} gives variational approximations to the exact bound energies. These energies will thus converge to the exact energies from above in the limit $\nu_{max} \to \infty$. Our bound-state energies are converged to at least three significant digits.

The bound-state energies calculated within these various approximations are summarized in Table III for the ^{4}He$_2$X systems with X = ^{6}Li, ^{7}Li, ^{23}Na, ^{39}K, ^{40}K, ^{41}K, ^{85}Rb, ^{87}Rb, and ^{133}Cs. We also include an estimate of the exact energy obtained by extrapolation (denoted $\nu_{max} \to \infty$). Extrapolation has been carried out by fitting the ν_{max}-dependent energies to $E_{\nu_{max}} = E_{exact} + \alpha/\nu_{max}^\beta$. To summarize, the ^{4}He$_2^6$Li and

^{4}He$_2^7$Li systems have each been found to possess two bound states ($n = 0$ and 1) for the $J^\Pi = 0^+$ symmetry and none for the other symmetries. The other ^{4}He$_2$X systems have been shown to support one bound state each for the $J^\Pi = 0^+$ and 1^- symmetries, and none for the $J \geqslant 2$ symmetries. In Table IV, the present results for the bound-state energies are compared with the previous results obtained using the hyperspherical adiabatic approximation [28,33], Faddeev [29], distributed Gaussian function [30,31], and diffusion Monte Carlo [32] approaches. The agreement between the present results and the previous calculations is found to be on only a qualitative level, even if the same combination of interaction potentials is used. We can see that binding energy calculations for these molecules are indeed very sensitive, depending upon the computational methods as well as on the potential models used. Specifically, our ^{4}He$_2^7$Li energy level obtained from the Li-He potential in Ref. [25] and the He-He potential in Ref. [1] disagrees with that of Baccarelli *et al.* [30,31] using the same potentials. Baccarelli *et al.* find a binding energy 14% bigger than ours, and we do not know the reason for this discrepancy. However, we are confident in our computational method, since it gives the bound-state energy of −14.31 mK for ^{4}He$_2^3$He [9], which agrees fairly well with the findings of Kolganova *et al.* [44], Nakaichi-Maeda and Lim [45], Roudnev [11], and Salci *et al.* [46], who obtained bound-state energies of −13.84, −13.66, −14.21, and −13.3 mK, respectively, employing diverse computational approaches but using the exact same He-He potential. Although these binding energies are smaller than that of He$_2$Li, the largest relative error with our result is still only half of that for He$_2$Li.

TABLE IV. Bound-state energies for the $^4\text{He}_2^6\text{Li}$, $^4\text{He}_2^7\text{Li}$, and $^4\text{He}_2^{23}\text{Na}$ systems, all in the $J^\Pi = 0^+$ symmetry. Energies are given in units of millikelvins and are relative to the three-body dissociation threshold. The present results (those with $\nu_{\max} \to \infty$) are compared with those calculated by Yuan and Lin [28] using the adiabatic hyperspherical approximation, Delfino *et al.* [29] using the Faddeev formalism, Baccarelli *et al.* [30,31] using the distributed Gaussian functions approach, Di Paola *et al.* [32] using the diffusion Monte Carlo method, and Li *et al.* [33] using the adiabatic hyperspherical approximation.

	$^4\text{He}_2^6\text{Li}$		$^4\text{He}_2^7\text{Li}$		$^4\text{He}_2^{23}\text{Na}$	$^4\text{He}_2^{39}\text{K}$
	$n = 0$	$n = 1$	$n = 0$	$n = 1$	$n = 0$	$n = 0$
This work	−58.88	−2.09	−81.29, −64.26[a]	−5.67, −3.01[a]	−152.68	−89.76
Reference [28]	−31.4[b]		−45.7[b]		−103.1[c]	
Reference [29]	−31.4[d]		−45.7[d]	−2.31[d]	−103.1[d]	
References [30], [31]	−53.4[a]	−7.9[a]	−73.4[a]	−12[a]		
Reference [32]			−57.1,[e] −65.0,[f] −80.0[g]		−119,[h] −148.5[i]	
Reference [33]						−66.6,[j] −115[k]

[a]Using the Li-He potential from Ref. [25] and the He-He potential from Ref. [1].
[b]Using the Li-He and He-He potentials from Ref. [26].
[c]Using the Na-He and He-He potentials from Ref. [26].
[d]Using a renormalized zero-range model.
[e]Using the Li-He and He-He potentials from Ref. [25].
[f]Using the Li-He potential from Ref. [27] and the He-He potential from Ref. [26].
[g]Using the Li-He potential from Ref. [27] and the He-He potential from Ref. [47].
[h]Using the Li-He potential from Ref. [27] and the He-He potential from Ref. [47].
[i]Using the Na-He potential from Ref. [27] and the He-He potential from Ref. [26].
[j]Estimation of the upper bound.
[k]Estimation of the lower bound.

A. $^4\text{He}_2^6\text{Li}$ and $^4\text{He}_2^7\text{Li}$ systems

The $^4\text{He}_2^6\text{Li}$ and $^4\text{He}_2^7\text{Li}$ systems possess bound states only for the $J^\Pi = 0^+$ symmetry, and none for the $J > 0$ symmetries. Figures 2(a) and 2(b) show the seven lowest $J^\Pi = 0^+$ adiabatic potential curves ($\nu = 0$–6) for the $^4\text{He}_2^6\text{Li}$ and $^4\text{He}_2^7\text{Li}$ systems, respectively, along with the bound-state energy levels. The effects due to the two different masses between ^6Li and ^7Li are shown here, and the potential curves for $^4\text{He}_2^7\text{Li}$ have a slightly deeper potential well than those for $^4\text{He}_2^6\text{Li}$. The energy levels for the heavier system ($^4\text{He}_2^7\text{Li}$) therefore lie at slightly lower energies than those for its lighter isotope ($^4\text{He}_2^6\text{Li}$). In Fig. 2(a), as $R \to \infty$, the lowest potential curve $\nu = 0$ approaches the $^4\text{He}_2 + {}^6\text{Li}$ dissociation threshold $E_{00}^{^4\text{He}_2} = -5.472 \times 10^{-9}$ a.u., and the second lowest one, $\nu = 1$, the $^4\text{He}^6\text{Li} + {}^4\text{He}$ dissociation threshold $E_{00}^{^4\text{He}^6\text{Li}} = -4.787 \times 10^{-9}$ a.u. In Fig. 2(b), as $R \to \infty$, the $\nu = 0$ potential curve approaches the $^4\text{He}^7\text{Li} + {}^4\text{He}$ dissociation threshold $E_{00}^{^4\text{He}^7\text{Li}} = -1.780 \times 10^{-8}$ a.u.; and the $\nu = 1$ potential, the $^4\text{He}_2 + {}^7\text{Li}$ dissociation threshold $E_{00}^{^4\text{He}_2} = -5.472 \times 10^{-9}$ a.u..

Figure 3 shows two-dimensional contour plots of the potential surface $V(R, \theta, \varphi)$ as well as the $\nu = 0$ and 1 channel functions for $^4\text{He}_2^6\text{Li}$ ($J^\Pi = 0^+$) at fixed hyperradii R, $R = 18.2$, 29.2, 60, and 640 a.u., as functions of the hyperangles θ and φ. The first R value, $R = 18.2$ a.u., corresponds to the minimum of the lowest potential curve $U_{\nu=0}(R)$, and the second one, $R = 29.2$ a.u., to the maximum of the first radial component $F_{\nu=0, n=0}(R)$ of the $n = 0$ state. The channel functions are plotted as $\sin 2\theta |\phi_{0\nu}|^2$, with $\phi_{0\nu}$ being the only component in the expansion of Φ_ν on the Wigner rotation matrices in Eq. (5). The maximum of $\sin 2\theta |\phi_{0\nu}|^2$ is found to correlate with the minimum of the potential surface at

a given value of R. At $R = 18.2$ a.u., the $\nu = 0$ channel function maximizes around $(\theta, \varphi) \approx (0.3\pi, \pi)$, for which the geometry of the triatomic system is a tall isosceles triangle,
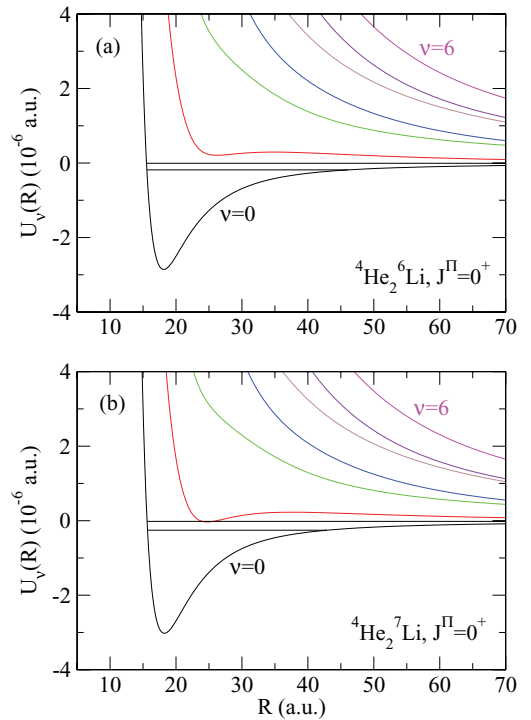

FIG. 2. (Color online) Adiabatic hyperspherical potential curves $U_\nu(R)$ as a function of the hyperradius R for (a) $^4\text{He}_2^6\text{Li}$ ($J^\Pi = 0^+$) and (b) $^4\text{He}_2^7\text{Li}$ ($J^\Pi = 1^-$). The seven lowest potential curves ($\nu = 0$–6) are shown, while the bound-state energies are indicated as horizontal lines.
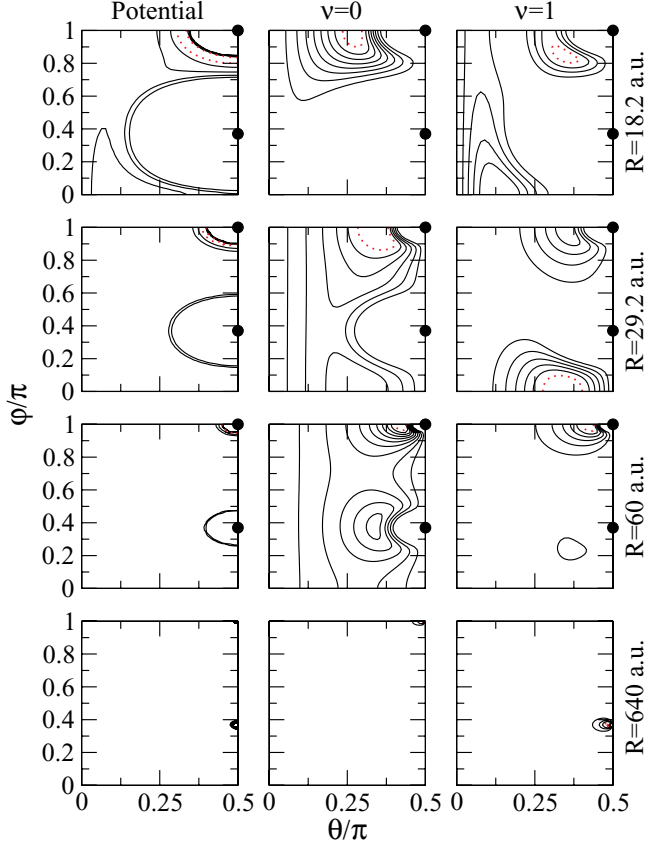
FIG. 3. (Color online) Two-dimensional contour plots of the potential surface $V(R,\theta,\varphi)$ (left column) and the $\nu = 0$ (middle column) and $\nu = 1$ (right column) channel functions plotted as $\sin 2\theta |\phi_{0\nu}|^2$ for $^4\text{He}_2^6\text{Li}$ ($J^\Pi = 0^+$) at four R values, as functions of the hyperangles θ and φ. The first row corresponds to $R = 19.2$ a.u.; the second row, to $R = 29.2$ a.u.; the third row, to $R = 60$ a.u.; and the fourth row, to $R = 640$ a.u.. The contour line of the potential surface with the lowest energy and that of the channel functions with the highest density are indicated by a dotted line. The $^4\text{He}\text{-}^6\text{Li}$ and $^4\text{He}\text{-}^4\text{He}$ coalescence points located respectively at $(\theta,\varphi) = (0.5\pi, 0.37\pi)$ and $(0.5\pi, \pi)$ are shown as filled circles (the lowest row excepted for visibility of the contour lines).

with ^6Li being at the top. As R increases, the maximum moves slowly toward larger values of θ along the line defined by $\varphi = \pi$. When R becomes much larger, it settles around

$(\theta,\varphi) \approx (\pi/2, \pi)$, representing a ^4He dimer and a ^6Li atom far away. The $\nu = 1$ channel function maximizes around $(\theta,\varphi) \approx (0.35\pi, 0.85\pi)$ for $R = 18.2$ a.u. but has a node around a line joining the points $(\theta,\varphi) \approx (0.15\pi, \pi)$ and $(0.35\pi, 0)$. At $R = 29.2$ a.u., however, the maximum switches to a point around $(\theta,\varphi) \approx (0.35\pi, 0)$, corresponding to a scalene triangle. When R becomes larger, it slowly approaches the point $(\theta,\varphi) = (\pi/2, 0.37\pi)$, corresponding to a $^4\text{He}_2^6\text{Li}$ molecule and a ^4He atom far away. The channel functions for the isotopic $^4\text{He}_2^7\text{Li}$ system are found to exhibit a behavior similar to that for the $^4\text{He}_2^6\text{Li}$ system.

For all of the $^4\text{He}_2^6\text{Li}$ and $^4\text{He}_2^7\text{Li}$ bound states, the $\nu = 0$ radial wave function, corresponding to the lowest channel, is found to dominate, while the second-lowest channel ($\nu = 1$) is the next dominant one. The contributions from the other channels are by far smaller. Quantitatively, we can define the occupation probability of channel ν in state n by $\int_0^\infty F_{n\nu}(R)^2 dR$. The occupation probabilities in the ground and excited states of $^4\text{He}_2^6\text{Li}$ and $^4\text{He}_2^7\text{Li}$ are reported in Table V. These are calculated including the six lowest channels in the coupled equations (6), or $\nu_{\max} = 5$. For all these states, the lowest channel, $\nu = 0$, dominates with a probability of more than 96%, while the second-lowest channel, $\nu = 1$, possesses a probability of less than about 3%. The higher channels contribute with probabilities of less than about 1%. However, as can be seen in Table III, the bound-state energy levels are still sensitive to the number of channels and are lowered significantly with further inclusion of channels.

The $\nu = 0$ radial wave function $F_{00}(R)$ of the $^4\text{He}_2^6\text{Li}$ ground state is found to peak at $R = 29.2$ a.u., for which, as shown in Fig. 3, the $\nu = 0$ channel function maximizes around $(\theta,\varphi) \approx (0.35\pi, \pi)$, in a tall isoceles triangle configuration. Therefore, using Eq. (10), this ground state can be thought of as exhibiting a tall isoceles triangle with $r_{12} = r_{31} \approx 25$ a.u. and $r_{23} \approx 7.8$ a.u. or, in other words, the ^4He dimer with the ^6Li atom a little loosely attached. The excited state of $^4\text{He}_2^6\text{Li}$ has its first radial component $F_{10}(R)$ peaking at a very large value of R, about $R \approx 200$ a.u., for which Φ_0 shows two ^4He atoms bound together and a ^6Li atom far away. This excited state thus displays essentially a ^6Li atom very loosely attached to a ^4He dimer, with the atom-molecule distance being about 200 a.u.. We have found similar $F_{n\nu}(R)$ for $^4\text{He}_2^7\text{Li}$, so this discussion should apply to it as well. Our determination of the molecular geometry is based on the position of the maxima of the

TABLE V. Occupation probabilities of the bound states for $^4\text{He}_2^6\text{Li}$, $^4\text{He}_2^7\text{Li}$, and $^4\text{He}_2^{23}\text{Na}$, calculated by including six channels ($\nu_{\max} = 5$).

| | $^4\text{He}_2^6\text{Li}$ | | $^4\text{He}_2^7\text{Li}$ | | $^4\text{He}_2^{23}\text{Na}$ | |
| | $J^\Pi = 0^+$ | | $J^\Pi = 0^+$ | | $J^\Pi = 0^+$ | $J^\Pi = 1^-$ |
ν	$n = 0$	$n = 1$	$n = 0$	$n = 1$	$n = 0$	$n = 0$
0	0.985	0.968	0.981	0.998	0.983	0.980
1	1.22×10^{-2}	3.01×10^{-2}	1.61×10^{-2}	1.55×10^{-3}	1.28×10^{-2}	1.68×10^{-2}
2	2.33×10^{-4}	1.47×10^{-3}	3.19×10^{-4}	3.95×10^{-4}	9.67×10^{-4}	1.46×10^{-3}
3	1.32×10^{-3}	2.62×10^{-5}	1.65×10^{-3}	1.22×10^{-5}	2.12×10^{-3}	2.32×10^{-4}
4	2.53×10^{-4}	3.12×10^{-5}	3.52×10^{-4}	1.34×10^{-5}	1.29×10^{-3}	2.96×10^{-4}
5	1.88×10^{-4}	7.47×10^{-6}	2.02×10^{-4}	1.28×10^{-5}	1.41×10^{-3}	8.80×10^{-4}

hyperangular probability distribution using Eq. (10) rather than on direct calculations of $\langle r_{ij} \rangle$. Our findings—$(r_{\text{LiHe}}, r_{\text{HeHe}}) \approx (25, 7.8)$ a.u. for the ground state and $r_{\text{HeHe}} \ll r_{\text{LiHe}} \approx 200$ a.u. for the excited state—are somewhat more qualitative than the geometries calculated by Baccarelli *et al.* [31]. They predict $(\langle r_{\text{LiHe}} \rangle, \langle r_{\text{HeHe}} \rangle) = (29.1, 23.1)$ a.u. and $(66.1, 88.4)$ a.u. for the $^4\text{He}_2^6\text{Li}$ ground and excited states, respectively. Although we do not expect quantitative agreement, our results differ from theirs already at qualitative level and predict quite different geometries for these states. Such disagreement, however, should probably be expected given the rather substantial differences in energies—even when the same interaction potentials are used. (Note that Ref. [31] gives a very detailed discussion of the dominant spatial configurations for $^4\text{He}_2^6\text{Li}$ and $^4\text{He}_2^7\text{Li}$.) The excited state of both $^4\text{He}_2^6\text{Li}$ and $^4\text{He}_2^7\text{Li}$ is found to extend to surprisingly large hyperradii R, especially for $^4\text{He}_2^7\text{Li}$, with its radial function F_{10} spreading over several thousands of atomic units. This might suggest that these molecules are among the largest triatomic molecules. The spatial extents of these excited states are found to be even larger than that of the $^4\text{He}_3$ excited state, and their binding energies are lower (for $^4\text{He}_3$ we obtained a binding energy of more than 1 mK for $^4\text{He}_3$ in Ref. [9]). Both of these excited states satisfy the condition $\langle R^2 \rangle / R_0^2 > 2$ (R_0 is the scaling parameter defined in Ref. [48]) to qualify as a halo state, since we find $\langle R^2 \rangle / R_0^2 \approx 130$ for $^4\text{He}_2^6\text{Li}$ and $\langle R^2 \rangle / R_0^2 \approx 700$ for $^4\text{He}_2^7\text{Li}$.

B. $^4\text{He}_2^{23}\text{Na}$ and other $^4\text{He}_2$–alkali-metal systems

The $^4\text{He}_2^{23}\text{Na}$ system is found to possess not only one bound state with $J^{\Pi} = 0^+$ but also one bound state with $J^{\Pi} = 1^-$. No bound state exists for the other symmetries. Figures 4(a) and 4(b) shows the seven lowest adiabatic potential curves ($\nu = 0$–6) of the $^4\text{He}_2^{23}\text{Na}$ system in the $J^{\Pi} = 0^+$ and 1^- symmetries, respectively. For a given ν, the potential curve in the 1^- symmetry is shallower than that in the 0^+ case. This is mainly due to additional terms amounting to $J(J+1)/2\mu R^2$ that appear in the Hamiltonian for $J \neq 0$. We can also see several avoided crossings between the 1^- potential curves.

Figure 5 shows two-dimensional contour plots of the potential surface $V(R, \theta, \varphi)$ and the $\nu = 0$ and 1 channel functions for $^4\text{He}_2^{23}\text{Na}(J^{\Pi} = 0^+)$ at fixed hyperradii $R = 20.0$, 26.4, 60, and 120 a.u., as functions of the hyperangles θ and φ. The first R value, $R = 20.0$ a.u., corresponds to the minimum of the lowest potential curve ($\nu = 0$), and the second one, $R = 26.4$ a.u., to the maximum of the $\nu = 0$ radial function of the ground state. These channel functions are plotted as $\sin 2\theta |\phi_{0\nu}|^2$. As was seen for $^4\text{He}_2^6\text{Li}$, the maximum of the probability distribution $\sin 2\theta |\phi_{0\nu}|^2$ correlates with the minimum of the potential surface at a given value of R, so that their behavior follows largely that described for $^4\text{He}_2\text{Li}$ too. At $R = 20.0$ a.u., for instance, the $\nu = 0$ channel function maximizes around $(\theta, \varphi) \approx (0.35\pi, \pi)$, where the triatomic system is a tall isosceles triangle with its top being ^{23}Na. When R becomes larger than 60 a.u., the maximum settles around $(\theta, \varphi) \approx (0.5\pi, 0.45\pi)$, displaying a $^4\text{He}^{23}\text{Na}$ molecule with a ^4He atom far away. The $\nu = 1$ channel function behaves
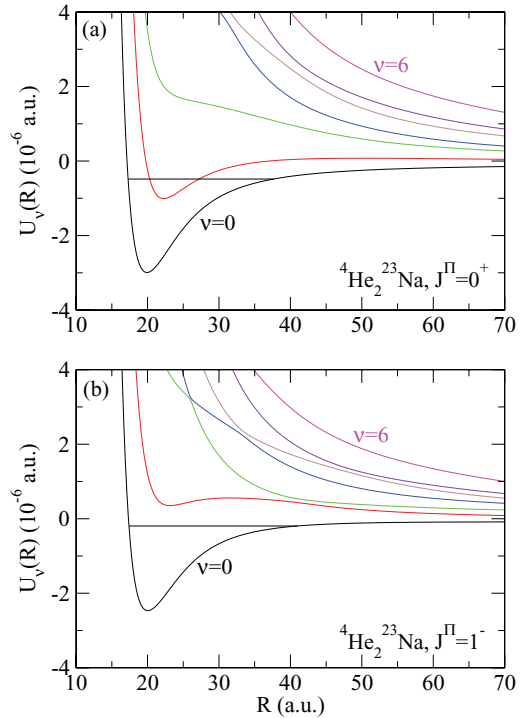

FIG. 4. (Color online) Adiabatic hyperspherical potential curves $U_\nu(R)$ as functions of the hyperradius R for $^4\text{He}_2^{23}\text{Na}$ in the (a) $J^{\Pi} = 0^+$ and (b) $J^{\Pi} = 1^-$ symmetries. The seven lowest potential curves ($\nu = 0$–6) are shown, while the bound-state energies are indicated as horizontal lines.

differently. At $R = 26.4$ a.u., the system becomes a scalene triangle, but at larger R, it shows a ^4He dimer and a ^{23}Na atom.

The $\nu = 0$ and 1 channel functions for $^4\text{He}_2^{23}\text{Na}$ ($J^{\Pi} = 1^-$) are found to behave in a similar manner. For the 1^- symmetry, there are two components, $K = -1$ and $K = +1$, in the expansion of the channel function on Wigner rotation matrices in Eq. (5), but because of the permutation symmetry we have $|\phi_{-1,\nu}|^2 = |\phi_{+1,\nu}|^2$. Hence, we only need to consider one of them. At small hyperradii R, the $\nu = 0$ channel function maximizes around $\theta = 0.25\pi \sim 0.4\pi$ and $\varphi = \pi$, for which the system is again an isosceles triangle. As R increases, the maximum of the channel function approaches $(\theta, \varphi) \approx (0.5\pi, 0.45\pi)$, corresponding to a $^4\text{He}^{23}\text{Na}$ molecule and a ^4He atom far away. The $\nu = 1$ channel function for $R = 20.0$ a.u. maximizes around $(\theta, \varphi) \approx (0.16\pi, 0)$, in a scalene triangle configuration, but as R increases its maximum approaches $(\theta, \varphi) \approx (0.5\pi, \pi)$, a ^4He dimer lying far away from a ^{23}Na atom.

For both of the $^4\text{He}_2^{23}\text{Na}$ bound states, the $\nu = 0$ radial wave function dominates over the other radial components. The occupation probabilities of these bound states calculated by including six channels (or $\nu_{\max} = 5$) are presented in Table V. For each state, the lowest channel contributes about 98%, the second-lowest channel just over 1%, and the other channels account for less than 1% all together. Combining these results, we conclude that the triatomic bound states for 0^+ and 1^- symmetries of $^4\text{He}_2^{23}\text{Na}$ are, like $^4\text{He}_2^6\text{Li}$, primarily a ^4He dimer, with the ^{23}Na atom relatively loosely attached.
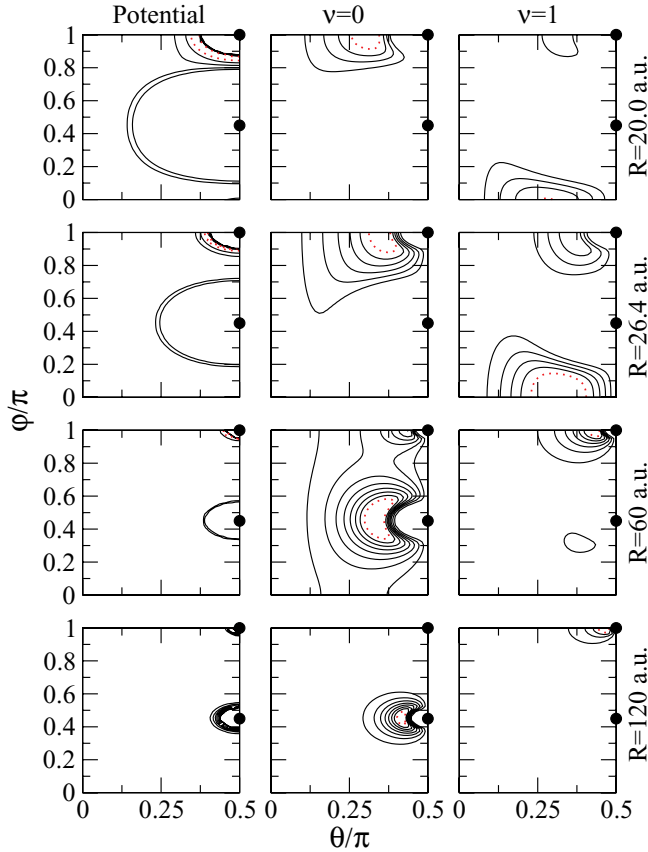
FIG. 5. (Color online) Two-dimensional contour plots of the potential surface $V(R,\theta,\varphi)$ (left column) and the $\nu = 0$ (middle column) and $\nu = 1$ (right column) channel functions plotted as $\sin 2\theta |\phi_{0\nu}|^2$ for ${}^4\mathrm{He}_2{}^{23}\mathrm{Na}(J^\Pi = 0^+)$ at four R values, as functions of the hyperangles θ and φ. The first row corresponds to $R = 20.0$ a.u.; the second row, to $R = 26.4$ a.u.; the third row, to $R = 60$ a.u.; and the fourth row, to $R = 120$ a.u.. The contour line of the potential surface with the lowest energy and that of the channel functions with the highest density are indicated by a dotted line. The ${}^4\mathrm{He}\text{-}{}^{23}\mathrm{Na}$ and ${}^4\mathrm{He}\text{-}{}^4\mathrm{He}$ coalescence points, located at $(\theta,\varphi) = (0.5\pi, 0.45\pi)$ and $(0.5\pi, \pi)$, respectively, are shown as filled circles.

We have also carried out calculations for the other ${}^4\mathrm{He}_2$–alkali-metal systems: ${}^4\mathrm{He}_2{}^{39}\mathrm{K}$, ${}^4\mathrm{He}_2{}^{40}\mathrm{K}$, ${}^4\mathrm{He}_2{}^{41}\mathrm{K}$, ${}^4\mathrm{He}_2{}^{87}\mathrm{Rb}$,

${}^4\mathrm{He}_2{}^{89}\mathrm{Rb}$, and ${}^4\mathrm{He}_2{}^{133}\mathrm{Cs}$. The adiabatic potential curves, channel functions, and radial functions are all qualitatively similar to those for ${}^4\mathrm{He}_2{}^{23}\mathrm{Na}$ just discussed.

IV. SUMMARY

In this work, we have studied the bound states for all ${}^4\mathrm{He}_2$–alkali-metal systems using the adiabatic hyperspherical representation. We have found two $J^\Pi = 0^+$ bound states for ${}^4\mathrm{He}_2{}^{6,7}\mathrm{Li}$ molecules, while one 0^+ and one 1^- bound state are found to exist for the other ${}^4\mathrm{He}_2$–alkali-metal molecules. We have also analyzed the adiabatic potential curves, channel functions, and radial wave functions to gain insight into the geometry of the molecules. We found that ${}^4\mathrm{He}_2{}^{6,7}\mathrm{Li}$ molecules in their excited states have a remarkably large spatial extent, among other things. It is important to note that the interaction potentials used in this work do not include retardation. To our knowledge, retardation corrections for HeX systems are not available. Retardation may have a significant effect and reduce the binding energies, as we found for the helium trimer and its isotopes [9].

In this work, we have not considered systems including the helium isotope ${}^3\mathrm{He}$, but it would be interesting to study ${}^3\mathrm{He}_2X$ and ${}^3\mathrm{He}{}^4\mathrm{He}X$. Although ${}^3\mathrm{He}$ cannot bind with an alkali-metal atom except for ${}^{23}\mathrm{Na}$, one can probably find three-body bound states for such systems, which would be Borromean states. The fermionic symmetry of ${}^3\mathrm{He}$ will no doubt be important. Finally, we want to note that this paper is the second in a sequence of three studying the system of ${}^4\mathrm{He}_2$ + alkali-metal atom. The first paper treated three-body recombination [37] and the third will treat atom-diatom processes [38]. All studies use the same pairwise potentials—in fact, they are all based on exactly the same adiabatic hyperspherical potentials and couplings.

ACKNOWLEDGMENTS

[1] R. A. Aziz and M. J. Slaman, J. Chem. Phys. **94**, 8047 (1991).

[2] R. A. Aziz, A. R. Janzen, and M. R. Moldover, Phys. Rev. Lett. **74**, 1586 (1995).

[3] M. Jeziorska, W. Cencek, B. Patkowski, B. Jeziorski, and K. Szalewicz, J. Chem. Phys. **127**, 124303 (2007).

[4] W. Cencek, M. Jeziorska, O. Akin-Ojo, and K. Szalewicz, J. Phys. Chem. A **111**, 11311 (2007).

[5] B. D. Esry, C. D. Lin, and C. H. Greene, Phys. Rev. A **54**, 394 (1996).

[6] D. Blume, C. H. Greene, and B. D. Esry, J. Chem. Phys. **113**, 2145 (2000).

[7] E. Nielsen, D. V. Fedorov, and A. S. Jensen, J. Phys. B **31**, 4085 (1998).

[8] R. Lazauskas and J. Carbonell, Phys. Rev. A **73**, 062717 (2006).

[9] H. Suno and B. D. Esry, Phys. Rev. A **78**, 062701 (2008).

[10] E. Nielsen and J. H. Macek, Phys. Rev. Lett. **83**, 1566 (1999).

[11] V. Roudnev, Chem. Phys. Lett. **367**, 95 (2003).

[12] A. K. Motovilov, W. Sandhas, S. A. Sofianos, and E. A. Kolganova, Eur. Phys. J. D **13**, 33 (2001).

[13] W. Sandhas, E. A. Kolganova, Y. K. Ho, and A. K. Motovilov, Few-Body Syst. **34**, 137 (2004).

[14] H. Suno, B. D. Esry, C. H. Greene, and J. P. Burke, Phys. Rev. A **65**, 042725 (2002).

[15] J. R. Shepard, Phys. Rev. A **75**, 062713 (2007).

[16] E. Braaten, H. W. Hammer, D. Kang, and L. Platter, Phys. Rev. A **78**, 043605 (2008).

[17] F. Luo, G. McBane, G. Kim, C. F. Giese, and W. R. Gentry, J. Chem. Phys. **98**, 3564 (1993).

[18] F. Luo, C. F. Giese, and W. R. Gentry, J. Chem. Phys. **104**, 1151 (1996).

[19] W. Schöllkopf and J. Toennies, Science **266**, 1345 (1994).

[20] W. Schöllkopf and J. Toennies, J. Chem. Phys. **104**, 1155 (1996).

[21] A. Kalinin, O. Kornilov, W. Schöllkopf, and J. P. Toennies, Phys. Rev. Lett. **95**, 113402 (2005).

[22] T. Havermeier *et al.*, Phys. Rev. Lett. **104**, 153401 (2010).

[23] T. Havermeier *et al.*, Phys. Rev. Lett. **104**, 133401 (2010).

[24] P. Dehmer and L. Wharton, J. Chem. Phys. **57**, 4821 (1972).

[25] D. Cvetko, A. Lansi, A. Morgante, F. Tommasini, P. Cortana, and M. G. Dondi, J. Chem. Phys. **100**, 2052 (1994).

[26] U. Kleinekathöfer, K. T. Tang, J. P. Toennies, and C. L. Yiu, Chem. Phys. Lett. **249**, 257 (1996).

[27] U. Kleinekathöfer, M. Lewerenz, and M. Mladenovi, Phys. Rev. Lett. **83**, 4717 (1999).

[28] J. Yuan and C. D. Lin, J. Phys. B **31**, L637 (1998).

[29] A. Delfino, T. Frederico, and L. Tomio, J. Chem. Phys. **113**, 7874 (2000).

[30] I. Baccarelli, G. Delgado Barrio, F. A. Gianturco, T. González-Lezana, S. Miret-Artes, and P. Villarreal, Phys. Chem. Chem. Phys. **2**, 4067 (2000).

[31] I. Baccarelli, G. Delgado, F. A. Gianturco, T. González-Lezana, S. Mirte-Artés, and P. Villarreal, Europhys. Lett. **50**, 567 (2000).

[32] C. Di Paola, F. A. Gianturco, F. Paesani, G. Delgado Barrio, S. Miret-Artés, P. Villarreal, I. Baccarelli, and T. González-Lezana, J. Phys. B **35**, 2643 (2002).

[33] Y. Li, Q. Gou, and T. Shi, Phys. Rev. A **74**, 032502 (2006).

[34] C. D. Lin, Phys. Rep. **257**, 1 (1995).

[35] B. R. Johnson, J. Chem. Phys. **73**, 5051 (1980).

[36] B. K. Kendrick, R. T. Pack, R. B. Walker, and E. F. Hayes, J. Chem. Phys. **110**, 6673 (1999).

[37] H. Suno and B. D. Esry, Phys. Rev. A **80**, 062702 (2009).

[38] H. Suno and B. Esry (in preparation).

[39] R. C. Whitten and F. T. Smith, J. Math. Phys. **9**, 1103 (1968).

[40] B. Lepetit, Z. Peng, and A. Kuppermann, Chem. Phys. Lett. **166**, 572 (1990).

[41] C. de Boor, *A Practical Guide to Splines* (Springer, New York, 1978).

[42] Visit the Web site, [http://www.nist.gov/pml/data/edi.cfm].

[43] B. D. Esry, C. H. Greene, and H. Suno, Phys. Rev. A **65**, 010705 (2001).

[44] E. A. Kolganova, A. K. Motovilov, and W. Sandhas, Phys. Part. Nuclei **40**, 206 (2009).

[45] S. Nakaichi-Maeda and T. K. Lim, Phys. Rev. A **28**, 692 (1983).

[46] M. Salci, E. Yarevsky, S. B. Levin, and N. Elander, Int. J. Quantum Chem. **107**, 464 (2007).

[47] K. T. Tang, J. P. Toennies, and C. L. Yiu, Phys. Rev. Lett. **74**, 1546 (1995).

[48] A. S. Jensen, K. Riisager, D. V. Fedorov, and E. Garrido, Rev. Mod. Phys. **76**, 215 (2004).